Caving 2018 – Y Potvin and J Jakubec (eds)

doi:10.36487/ACG_rep/1815_42_de_Beer

Towards physics-based hazard assessment tools for developing blanket re-entry rules

W de Beer *ESG Solutions, Canada*

L Smith-Boughner *ESG Solutions, Canada*

G Viegas *ESG Solutions, Canada*

K Bosman *ESG Solutions, Canada*

D Angus *ESG Solutions, Canada*

Abstract

Hazard assessment tools are often classified as either purely probabilistic or deterministic. Probabilistic assessments utilise the statistics of past occurrences to attempt a forecast, with suitable confidence levels, of future occurrences in a given spatial volume and time frame. Purely deterministic methods use constitutive equations, equations of state, or equations of motion to extrapolate future behaviour.

In this paper, we report on initial work towards deterministic assessments by compiling the statistics of the behaviour of physical variables based on seismic source parameters, and rock mass stress state and condition inferred from seismic velocities for comparison to the occurrence of significant events and/or damage at particular locations in mines.

At this stage, we only report on whether patterns and statistics may exist.

Keywords: *passive seismic tomography, seismic velocity, seismic time series*

1 Introduction

Routine weekly passive seismic tomography is performed at a block caving mine. The tomography forms part of a basket of monitoring techniques which is used to assist in the management of the rock mass response to mining.

At the time of writing, more than one year of weekly snapshots (see Figure 1 for a small example) of modelled three-dimensional distribution of P- and S-wave velocities (denoted V_P and V_S, respectively, and seismic velocities collectively) have been accumulated. This dataset is becoming of sufficient size that it could begin to be exploited, in conjunction with other data, for hazard assessment, and in particular for establishing rules for re-entry into an area following large events or blasting.

One line of enquiry is into possible relationships between changes in seismic velocities and damage (seismic hammering), or the occurrence of damaging events or flurries of events. In areas where this is consistently the case, considering the behaviour of seismic velocities in addition to the usual decay rates (Malek & Leslie 2006; Vallejos & McKinnon 2011) may enhance risk management.

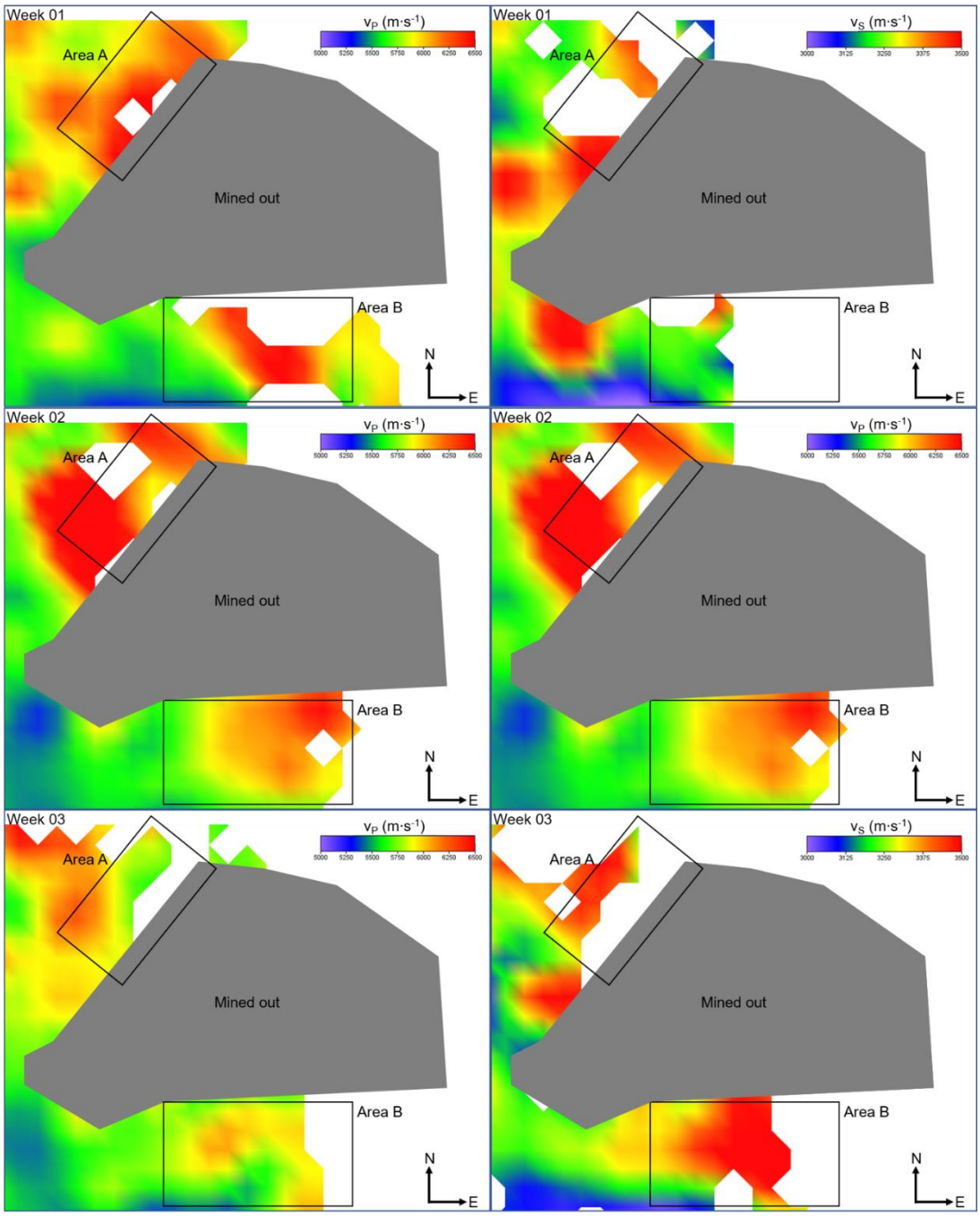

Figure 1 Evolution of modelled P- and S-wave velocities on a cut plane through the production level. The rectangular boxes delineate the two sampled areas of the mine, Area A and Area B

V_P is a combination of bulk and shear modulus normalised by material density, and V_S is shear modulus normalised by material density. Areas of increasing stress should show increasing velocities. Increasing stress translates to closing joints, fractures and microcracks (grain boundaries of rock) and to the increasing stiffness of the rock. Conversely, areas of decreasing velocities can be interpreted as destressing and/or post-peak rock failure. The sensitivity of body wave velocity to stress varies from approximately 0.1 to 1% change in velocity per change in MPa (Niu et al. 2008; Silver et al. 2007; Yamamura et al. 2003). Thus, a stress variation of 10 MPa would yield deviation from the background velocity ranging from 1 to 10%. A very tentative classification of the state of the rock mass based on these ideas is shown in Table 1.

Table 1 Tentative classification scheme mapping seismic velocity to stress, stiffness, and state of the rock mass

State	V_P/stress	V_S/stiffness
Brittle	High	High
Moderately brittle (stress accumulation)	High moderate	Moderate high
Plastic (potential for large deformation for small stress increments)	High	Low
Stable	Low	High
Yielded	Low	Low

This paper describes the initial exploration of correlations between the tomography and more conventional seismic variables used for stability and hazard assessments. In particular, the cumulative scalar seismic moment (ΣM_0) and the energy index (EI) are considered. The scalar seismic moment is a proxy for co-seismic deformation, since it can be written as $M_0 = \mu[u]A$, where μ is the shear modulus of the rock, $[u]$ is the mean displacement during rupture, and A is the rupture area (see for example Aki & Richards 2002). The EI is a proxy for (shear) stress release at the source of a seismic event (see for example Mendecki 1996). It is defined as the ratio of the seismic energy E_S radiated by an event and the seismic energy expected to be radiated by events with the same scalar seismic moment. The expected energy is determined by fitting a line through a scatterplot of $\log_{10} E_S$ and $\log_{10} M_0$.

2 Data

Seismic data was sampled from two areas of the mine (Figure 1). Area A is a competent, largely unmined abutment containing a diorite–hornfels contact. Area B also contains a diorite–hornfels contact, but has been mined in the sense that it is an area with pillars and drives. Both areas measure approximately 200 m long, 150 m wide and 120 m thick. Approximately 18 months of data was used in the analysis. The minimum magnitude of completeness in both areas over this period is M_W -1, so only events of this magnitude or more were used.

Area A did not experience any excessively large events ($M_W \geq 2$) in this period, although from late in month 03, after the occurrence of an M_W 2.7 event in Area B, adjacent areas have regularly experienced events in the range of $0.5 \geq M_W \geq 1$, influencing seismicity rates in the area. There were, however, two episodes of accelerated seismic release. Area B, on the other hand, is prone to larger events ($M_W > 1.5$) with little precursory activity. Both areas often show high P-wave and high S-wave velocities.

3 Methodology

3.1 Comparative results

Time series of the maximum weekly seismic velocities, cumulative scalar seismic moment, and median EI in each area were constructed. For most of the time period under consideration, the velocities were calculated once a week (mostly for the seven days Monday to Sunday inclusive), but for the last month, this changed to thrice weekly; Monday to Sunday (inclusive), Wednesday to Tuesday (inclusive), and Friday to Thursday (inclusive). The effect of the higher time resolution will be the subject of subsequent papers. The behaviour of the time series within the areas was studied, and the series were compared and contrasted between the areas.

3.2 Passive tomography

Measured travel times of seismic signals (microseismic events and blasts) from source–sensor pairs are used for travel time tomography to image seismic velocities in the rock volume sampled by the source–sensor paths. The rock is discretised into a grid of 3D volume elements and ray path segments associated with the volume in which they occur. Velocity perturbations are determined for grid cells with sufficient ray coverage. As a starting velocity model, a 1D background velocity (half space) is used and perturbed to generate a 3D velocity model. Initial inputs consist of using blasts and microseismic events for a grid of volume elements as obtained through travel time tomography. Continued tracking of velocity changes uses the ray paths of subsequent blasts and microseismic events. Our approach is based on a variant of the simultaneous iterative reconstruction technique (SIRT; see Crowley et al. 2015; Baig et al. 2017), which performs each inversion rapidly by a series of iterative updates. At each iteration, the travel time residual for a given ray path in the velocity model found in the previous iteration is distributed amongst the grid cells that the ray intersects. An algebraic formulation for the velocity in each grid cell can then be evaluated, avoiding the need to explicitly invert a large system of equations, and thus providing a computationally efficient inversion algorithm.

The example presented here assumes an isotropic velocity model. Our implementation of the SIRT method is able to account for vertical transverse isotropy (VTI) but requires a priori information about the degree of anisotropy, which was not available for this example. The background velocity in the area of interest can be considered relatively uniform, so we have used a straight ray path approximation. We have excluded ray paths which pass through the caved volume, where straight ray paths are clearly not appropriate. It is possible to model the first arrival times for such ray paths with a fast marching eikonal solver (Rawlinson & Sambridge 2005), but in practice we find that the observed waveform complexity indicates that such paths are not well-modelled by the ray approximation. As a result, we exclude these complex ray paths to minimise the errors introduced into the velocity inversion.

3.3 Resolution tests

For tomography, it is generally understood that volumes rich in ray paths crossing from different trajectories result in better resolution as compared to volumes where ray paths originate from a single direction. At the time the data used in this paper was acquired, the central and western parts of the mine were well-covered by the array, providing a dense crossing of rays to enable a robust determination of velocities in these regions. To understand the effects of resolution imposed by the ray geometry on the calculated velocities more succinctly, a checkerboard test is used; see Rawlinson and Sambridge (2003) for a discussion of this methodology. The test consists of a synthetic model of travel times with alternating blocks of high and low velocities. When these synthetic travel times are inverted, areas that recover the input synthetic model are said to be well-resolved, and the smearing effects of poorly constraining ray geometry is also observed in the recovered images. To further test the robustness of the inversions, random arrival time picking errors are added to the input travel times.

3.4 Seismic time series

Calculation of the seismic time series of interest was standard. The logarithm (base 10) of the EI was used, and it was additionally smoothed by taking the median over 10 data points in a period of at least 24 hours.

4 Results

Initial results are shown in Figures 2 to 5. Note that care was taken to have the same ranges on the same axes for each area in order to facilitate comparisons. Some observations are in order. First, it appears that where the time scale of changes in seismic variables and velocities are comparable, there are concurrent changes in the velocities. For most of the time, the velocities are binned in week-long periods, so their responses are low resolution. Second, the response in the EI is weak, which could indicate that more optimisation is required. The EI is well-known to be sensitive to fluctuations. The time window over which the median is taken, or the fall-back number of data points, requires careful calibration for each area to minimise fluctuations, but at the same time not induce aliasing or over-smoothing.

In Area A (Figure 2), the comparative responses show that, in one case, as the deformation increases over several days, there appears to be an increase in ambient stress (as encoded in the P-wave velocity), supported by the EI showing a decreasing trend. This makes sense if one considers that less and less stress is released by seismic deformation while stress is stored in the surrounding rock mass.

Area B (Figure 3) is very different. The P-wave velocity behaviour has the appearance of stress cycling between deformation episodes. The seismic deformation due to the two large events occurred suddenly, at too high a temporal resolution for the week-long velocity window. However, in the latter six weeks or so of the time series, when there is a three-fold increase in the temporal resolution of the seismic velocity data, there is a suggestive similarity in the behaviour of the seismic velocities and the EI.

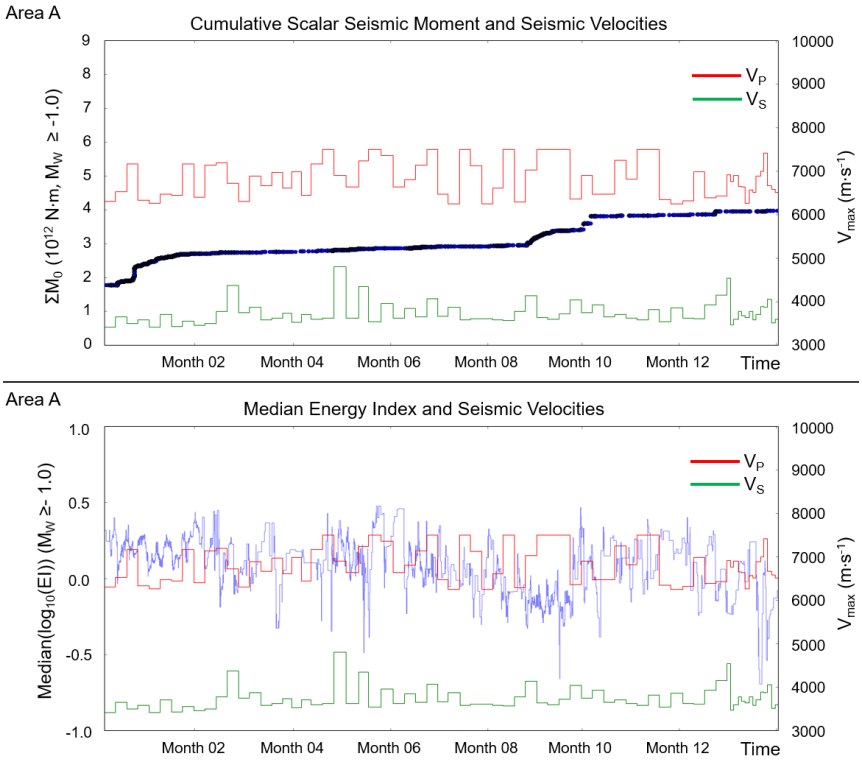

Figure 2 Cumulative scalar seismic moment (top) and median EI (bottom) in Area A, plotted on the same graphs as the maximum P-wave velocity and maximum S-wave velocity. Axis ranges were kept the same for the two areas to facilitate comparison

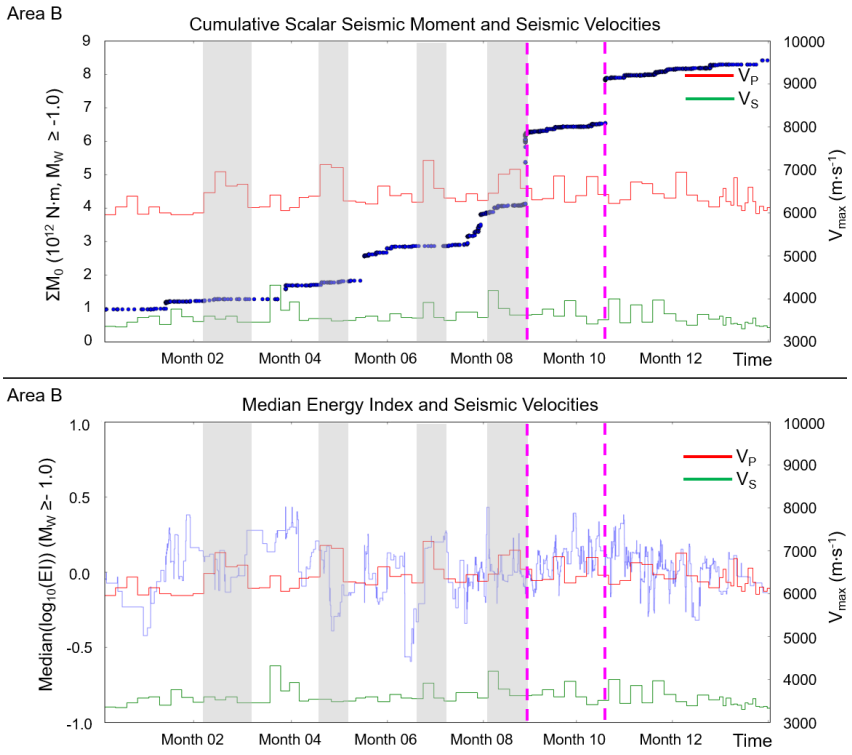

Figure 3 Cumulative scalar seismic moment (top) and median EI (bottom) in Area B, plotted on the same graphs as the maximum P-wave velocity and maximum S-wave velocity. Axis ranges were kept the same for the two areas to facilitate comparison. Grey rectangles highlight significant excursions in P-wave velocity. Dashed vertical magenta lines indicate times of occurrence of large ($M_W \geq 2$) events

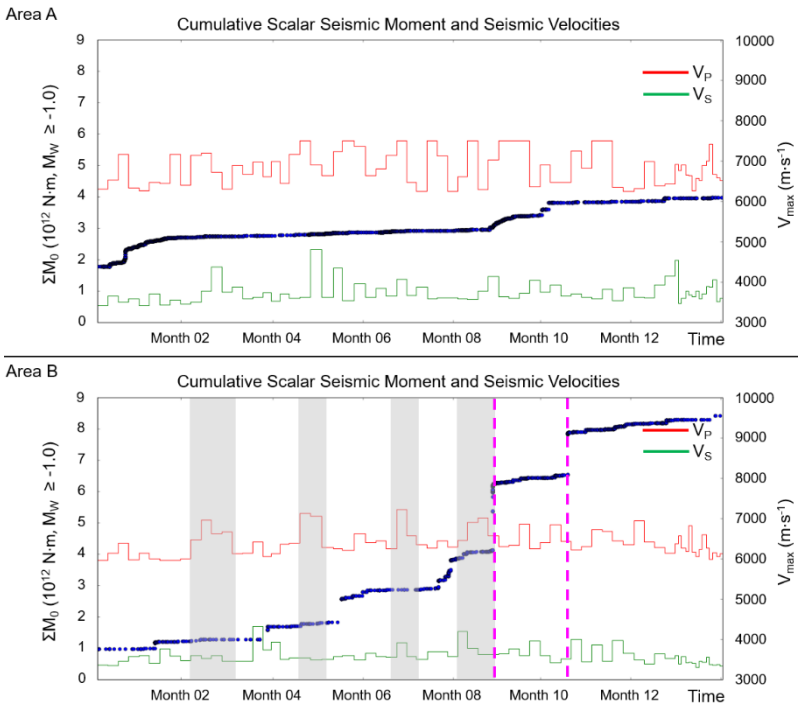

Figure 4 Cumulative scalar seismic moment in Area A (top) and Area B (bottom), plotted on the same graphs as the maximum P-wave velocity and maximum S-wave velocity. Axis ranges were kept the same for the two areas to facilitate comparison. Grey rectangles highlight significant excursions in the P-wave velocity. Dashed vertical magenta lines indicate times of occurrence of large ($M_W \sim 2 \pm 0.2$) events

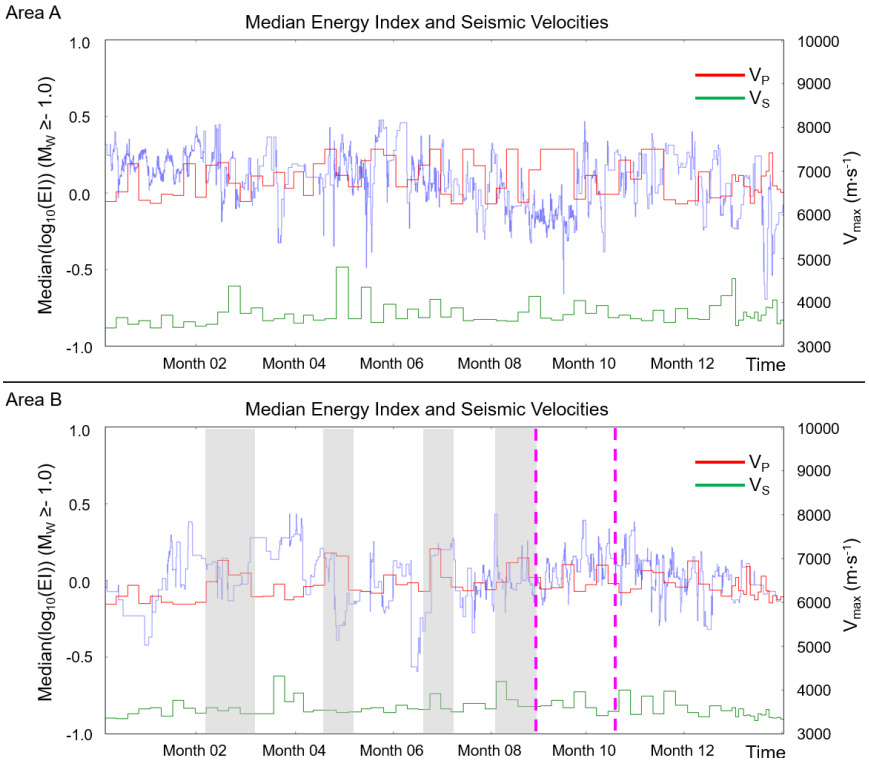

Figure 5 Median EI in Area A (top) and in Area B (bottom), plotted on the same graphs as the maximum P-wave velocity and maximum S-wave velocity. Axis ranges were kept the same for the two areas to facilitate comparison. Top: grey rectangles highlight times of accelerated moment release; Bottom: dashed vertical magenta lines indicate times of occurrence of large (M_W ~ 2 ± 0.2) events

5 Conclusion

More than one year's worth of weekly passive seismic tomography inversions at a block caving mine were compared to time series of seismic release as described by the cumulative scalar seismic moment and the median (log base 10) EI. In the cases where the seismic variables change on a time scale comparable to the velocities, the responses in these variables were concurrent. One of the areas considered shows an intriguing stress cycling type behaviour, punctuated by sudden large changes in seismic moment (the occurrence of larger events).

The time window over which the seismic velocities are inverted is a function mainly of data density and computing power. The seismic velocities have a very direct physical interpretation; the last few weeks of the time series show that if the time resolution of routine inversions could be increased, and the comparative analyses and distribution of results automated, they can be a useful addition to the basket of properties and trends used for day-to-day hazard assessment.

References

Aki, R & Richards, PG 2002, *Quantitative Seismology*, 2nd edn, University Science Books, Sausalito.

Baig, AM, Bosman, K & Urbancic, TI 2017, 'Temporal changes in stress state imaged through seismic tomography', in J Wesseloo (ed.), *Proceedings of the Eighth International Conference on Deep and High Stress Mining*, vol. 1, Australian Centre for Geomechanics, Perth, pp. 269–273.

Crowley, JW, Baig, AM, Urbancic, TI & von Lunen, E 2015, '4D tomography and deformation from microseismic data', *Proceedings of the 85th Annual Meeting of the Society of Exploration Geophysics*, Society of Exploration Geophysicists, Tulsa.

Malek, F & Leslie, IS 2006, 'Using seismic data for rockburst re-entry protocol ant INCO's Copper Cliff North Mine', in D Yale, S Holtz, C Breeds & U Ozbay (eds), *Proceedings of the 41st Symposium on Rock Mechanics: 50 Years of Rock Mechanics – Landmarks and Future Challenges*, American Rock Mechanics Association, Alexandria.

Mendecki, AM 1996, *Quantitative Seismology in Mines*, Springer, Basel.

Niu, F, Silver, PG, Daley, TM, Cheng, X & Majer, EL 2008, 'Preseismic velocity changes observed from active source monitoring at the Parkfield SAFOD drill site', *Nature*, vol. 454, pp. 204–208.

Rawlinson, N & Sambridge, M 2003, 'Seismic traveltime tomography of the crust and lithosphere', *Advances in Geophysics*, vol. 46, pp. 81–198.

Rawlinson, N & Sambridge, M 2005, 'The fast marching method: an effective tool for tomographic imaging and tracking multiple phases in complex layered media', *Exploration Geophysics*, vol. 36, pp. 341–350.

Silver, PG, Daley TM, Niu F & Majer, EL 2007, 'Active source monitoring of crosswell seismic travel time for stress-induced changes', *Bulletin of the Seismological Society of America*, vol. 97, no. 1, 281–293.

Vallejos, JA & McKinnon, SD 2011, 'Correlations between mining and seismicity for re-entry protocol development', *International Journal of Rock Mechanics and Mining Sciences*, vol. 48, no. 4, pp. 616–625.

Yamamura, K, Sano, O, Utada, H, Takei, Y, Shigeru, N & Fukao, Y 2003, 'Long-term observation of in situ seismic velocity and attenuation', *Journal of Geophysical Research*, vol. 108, pp. 2317–2331.